

# Manganites at Quarter Filling: Role of Jahn-Teller Interactions

Jan Bała

Max-Planck-Institut für Festkörperforschung, Heisenbergstrasse 1,

D-70569 Stuttgart, Federal Republic of Germany and

Institute of Physics, Jagellonian University, Reymonta 4, PL-30059 Kraków, Poland

Peter Horsch and Frank Mack

Max-Planck-Institut für Festkörperforschung, Heisenbergstrasse 1,

D-70569 Stuttgart, Federal Republic of Germany

(Dated: May 22, 2019)

We have analyzed different correlation functions in a realistic spin-orbital model for half-doped manganites. Using a finite-temperature diagonalization technique the CE phase was found in the charge-ordered phase in the case of small antiferromagnetic interactions between  $t_{2g}$  electrons. It is shown that the dominant mechanism responsible for stabilization of the CE-type spin and orbital-ordered state is the cooperative Jahn-Teller (JT) interaction between next-nearest  $\text{Mn}^{+3}$  neighbors mediated by the breathing mode distortion of  $\text{Mn}^{+4}$  octahedra and displacements of  $\text{Mn}^{+4}$  ions. The topological phase factor in the Mn-Mn hopping leading to gap formation in one-dimensional models for the CE phase as well as the nearest neighbor JT coupling are not able to produce the zigzag chains typical for the CE phase in our model.

PACS numbers: 75.30.Kz, 71.70.Ej, 75.30.Et, 75.10.-b

## I. INTRODUCTION

Half-doped perovskite manganites  $\text{Re}_{1/2}\text{A}_{1/2}\text{MnO}_3$  (Re=rare earth, A=alkaline earth) exhibit very specific properties quite different from manganites with other  $e_g$  electron concentrations.<sup>1,2</sup> Generally, for large size Re and A cations or when external pressure is applied<sup>3</sup> these compounds are in the A-type antiferromagnetic (AF), metallic state at low temperatures showing no or only weak sign of charge ordering, and the occupied  $e_g$  electron states are predominantly  $x^2-y^2$  like. Recently it has been reported that the A-phase may develop an intrinsic charge-stripe modulation, which controls the transport properties.<sup>4</sup> With decreasing size of the cations, which implies a decrease of the bandwidth, charge ordering is observed which at lower temperatures is accompanied by the formation of peculiar ferromagnetic (FM) zigzag chains<sup>5,6,7</sup> that are staggered antiferromagnetically. This charge-exchange (CE) spin order is accompanied by a checkerboard charge order (CO) and directed occupied orbitals on the  $\text{Mn}^{3+}$  sites amplifying double exchange along one lattice diagonal. The CE-structure is a particularly fascinating manifestation of the control of magnetic order due the orbital degree of freedom<sup>8</sup> in combination with charge ordering. Although, the CE spin-orbital<sup>9</sup> order has been described already in the seminal works of Goodenough<sup>10</sup> and of Wollan and Koehler<sup>11</sup> the mechanism for its stability is still not clear and hotly debated with emphasis put on the role of the double-exchange (DE),<sup>12,13,14</sup> the Coulomb interaction,<sup>15,16,17,18</sup> or the coupling to the lattice degrees of freedom.<sup>19,20,21,22,23</sup>

The CE phase has been observed experimentally both in cubic  $(\text{Nd,Pr})_{1/2}(\text{Sr,Ca})_{1/2}\text{MnO}_3$ <sup>2,7,24,25,26</sup> and in layered  $\text{LaSr}_2\text{Mn}_2\text{O}_7$ <sup>27</sup> and  $\text{La}_{1/2}\text{Sr}_{3/2}\text{MnO}_4$ <sup>5,6</sup> manganites. In some cases it can coexist with the A-type AF spin

ordering.<sup>27,28,29</sup> Regarding CO in the CE phase, some experiments are interpreted in terms of almost perfect CO<sup>6,30</sup> while others<sup>31</sup> are considered to be consistent with a smooth charge density wave (CDW) of the  $e_g$  electrons. Although, it is plausible that the complex spin and orbital arrangement in the charge-ordered manganites can result from the competition between DE<sup>32</sup> and AF superexchange interactions ( $\sim J_{\text{AF}}$ ), the role played by the CO and Jahn-Teller (JT) interactions<sup>20,21,22,33</sup> in the system is still unclear. Finally in systems like e.g.  $\text{Pr}_{1/2}\text{Ca}_{1/2}\text{MnO}_3$  CO and CE-type orbital correlations are found to develop well above the Neel temperature<sup>34,35</sup> or even coexist with FM spin state<sup>36</sup>, which indicates that these orbital correlations are not primarily driven by magnetic interactions.

This work focuses on a microscopic understanding of the stability of the CE-phase which appears to be the ground state of narrow band manganites at and near quarter-filling. We argue here that the key interaction, apart from the nearest-neighbor Coulomb repulsion  $V$  which supports the charge ordering,<sup>37</sup> is the next-nearest neighbor JT interaction. This interaction between orbitals at next-nearest neighbor  $\text{Mn}^{3+}$  ions emerges from the JT-distortions of the  $\text{Mn}^{3+}$  octahedra which is amplified by the breathing distortion of the intermediate  $\text{Mn}^{4+}$  octahedra. We show that this interaction generates a narrow regime in the  $V-J_{\text{AF}}$  phase diagram where the CE-phase (and sometimes the C-phase) is stable. Otherwise one encounters a homogeneous ferromagnetic phase at small  $J_{\text{AF}}$  fully controlled by DE and a conventional nearest-neighbor antiferromagnetic phase at larger  $J_{\text{AF}}$ .

An important feature of this mechanism are the displacements of the  $\text{Mn}^{4+}$  ions. We are only aware of work by Radaelli *et al.*<sup>38</sup> where detailed lattice coordinates for the CE-phase in  $\text{La}_{1/2}\text{Ca}_{1/2}\text{MnO}_3$  are reported. In par-

ticular they observed that the 4 planar O(2) move towards the Mn<sup>4+</sup> ion and the Mn<sup>4+</sup> ions are found to be displaced from their regular perovskite positions, while the Mn<sup>3+</sup> ions are not shifted. This observation confirms the importance of the breathing distortion and also shows the mechanism of the further neighbor JT-distortion in the CE-phase. As a consequence the appearance of new Bragg reflections in the CE-phase would be associated not primarily with quadrupolar electronic OO but rather with the displacements of ions associated with the CE orbital order.<sup>38</sup>

An alternative long-ranged JT based interaction was recently proposed by Khomskii and Kugel<sup>39</sup> and by Calderon, Millis and Ahn.<sup>40</sup> They employ elasticity theory to derive the orbital interaction between JT-distorted Mn<sup>3+</sup>O<sub>6</sub> octahedra for the perfectly charge ordered case. We have also investigated the consequences of this interaction. Our numerical simulations confirm the estimate presented in Ref.39 that for perfect charge ordering the AF CE phase is stable. Yet in this model this requires large nearest neighbor Coulomb repulsion  $V$ , while for moderate values of  $V$  the CE phase gets unstable.

The finite temperature diagonalization<sup>16,41,42</sup> used in our study allows to include the full interplay of spin and orbital states, and to monitor the onset of different orders as function of temperature. This gives us the ability for an unbiased investigation of the formation of different spin-orbital orderings emerging from all multi-electron configurations in the cluster. In this paper we concentrate on the stability and temperature dependence of spin, orbital, and charge ordered states in the two-dimensional (2D) realistic model for half-doped manganites. In our microscopic spin-orbital model CO develops as a result of nearest-neighbor Coulomb repulsion  $V$  and as a consequence of further neighbor JT interactions, while the spin-orbital order results from the competition between double exchange (i.e. kinetic energy), antiferromagnetic superexchange and further neighbor JT interactions. As shown in Sec. IIID the latter interaction can lead to a CO state at low temperatures even in the absence of Coulomb repulsion. Furthermore we argue that a topological sign in the hopping amplitudes of  $e_g$  orbitals<sup>13</sup> invoked in one-dimensional (1D) models for the CE phase is not sufficient to explain the formation of CE spin-orbital structure in the 2D model studied by us.

Further motivations to put effort in a better understanding of the interplay of spin, charge, orbitals and lattice in the formation of the CE-phase are the following: It has been argued that the intrinsic mechanism that leads to colossal magnetoresistance are tendencies towards CE-type charge and orbital ordering in the vicinity of  $x = 0.5$ .<sup>43</sup> Furthermore a CE-insulator to FM-metal transition has been observed in relatively small magnetic field, which is accompanied by a major change of the optical conductivity on a surprisingly large energy scale ( $\sim 1$  eV).<sup>44,45</sup> Such dramatic changes in relatively weak magnetic fields are a clear manifestation of the subtle interplay between spin, orbital and charge order. The

present study provides a basis for further investigations of the temperature dependence of e.g. the optical conductivity and the study of spin and orbital excitations in the CE-phase, as well as the effect of doping into the quarter filled state.

The paper is organized as follows. In Sec. II we present the model Hamiltonian, and describe in Sec. IIIB the finite-temperature Lanczos method. Sec. III contains numerical results for different two-site correlation functions characterizing the charge, orbital and spin structure. These correlation functions are evaluated as functions of temperature and collected in a form of semi-quantitative phase diagrams in three different regimes: (i) including nearest-neighbor effective orbital-orbital (OO) interactions (Sec. IIIC); (ii) assuming the elastic form of OO coupling at different distances (Sec. IIID); (iii) considering the local form of next- and nearest-neighbor OO coupling (Sec. IIIE), while in Sec. IIIF the effect of charge stacking is discussed. The paper is summarized in Sec. IV. In the Appendix the stability of the CE versus the C phase is analysed for a 1D band model with lifted orbital degeneracy.

## II. MODEL HAMILTONIAN AND NUMERICAL PROCEDURE

### A. Effective spin-orbital model

We consider the generic FM Kondo lattice model for manganites<sup>41,42</sup> with the Mn  $e_g$  electrons coupled to the core  $t_{2g}$  spins via the Hund coupling  $J_H$ . The model is augmented by inter-site Coulomb repulsion  $V$  and cooperative JT interactions and treated in the limit of infinite on-site Coulomb repulsion between two  $e_g$  electrons on the same site ( $U \rightarrow \infty$ ):

$$H = H_{band} + H_{Kondo} + H_{AF} + H_V + H_{OO}. \quad (1)$$

The first term describes the motion of the  $e_g$  electrons,

$$H_{band} = - \sum_{\langle ij \rangle \xi \zeta, \sigma} \left( t_{ij}^{\xi \zeta} \tilde{d}_{i\xi\sigma}^\dagger \tilde{d}_{j\zeta\sigma} + \text{H.c.} \right), \quad (2)$$

with a constraint that allows only for Mn<sup>4+</sup> and Mn<sup>3+</sup> configurations,  $\tilde{d}_{i\xi\sigma}^\dagger = d_{i\xi\sigma}^\dagger (1 - n_{i\xi\bar{\sigma}}) \prod_{\sigma'} (1 - n_{i\xi\sigma'})$ , where all other alternative  $e_g$  states are projected out. Here and in the following the index  $\bar{\xi}$  ( $\bar{\sigma}$ ) denotes the  $e_g$  orbital (spin) orthogonal to the  $\xi$  ( $\sigma$ ) one, respectively. The hopping matrix elements depend on the basis chosen. For the basis  $\{|x\rangle, |z\rangle\}$  with  $|x\rangle \sim x^2 - y^2$  and  $|z\rangle \sim 3z^2 - r^2$  they are given by,

$$\left[ t_{ij||a(b)}^{\xi \zeta} \right] = \frac{t}{4} \begin{pmatrix} 3 & \mp\sqrt{3} \\ \mp\sqrt{3} & 1 \end{pmatrix}, \quad (3)$$

where,  $+$  ( $-$ ) refer to the  $a$  ( $b$ ) direction, respectively. The second term of Hamiltonian (1) stands for the Hund interaction between  $e_g$  electrons spin and the  $S = 3/2$   $t_{2g}$

core spin  $\mathbf{S}_i$ ,

$$H_{Kondo} = -J_H \sum_{\langle ij \rangle \xi \sigma \sigma'} \mathbf{S}_i \cdot \tilde{d}_{i\xi\sigma}^\dagger \tilde{\sigma}_{\sigma\sigma'} \tilde{d}_{i\xi\sigma'}, \quad (4)$$

resulting in the parallel alignment of spins between  $t_{2g}$  and  $e_g$  electrons at each site in the limit  $J_H \gg t$  which corresponds to the realistic situation in manganites. The  $H_{band} + H_{Kondo}$  part of the total Hamiltonian alone represents the DE mechanism and yields a FM ground state with  $|x\rangle$  orbitals being occupied which is favored by the kinetic energy in 2D model. Such a fully spin polarized case at finite  $U$  leads to *the orbital t-J model* as considered in Refs. 41,42. Here, we are interested in the more complex case where both spin and orbital degrees of freedom play an active role. Therefore, an AF ( $J_{AF} > 0$ ) coupling between nearest-neighbor  $t_{2g}$  spins is also incorporated,

$$H_{AF} = J_{AF} \sum_{\langle ij \rangle} \mathbf{S}_i \cdot \mathbf{S}_j. \quad (5)$$

In our numerical studies we assume  $S = 1/2$  for the core spins which decreases the resulting Hilbert space considerably. We have tested that this assumption gives similar results as in the  $S = 3/2$  case when  $J_H$  is renormalized<sup>46</sup> by the factor 3. Moreover, to promote the charge ordering as observed experimentally in half-doped manganites we include the Coulomb repulsion ( $V > 0$ ) between  $e_g$  electrons on neighboring sites,<sup>46</sup>

$$H_V = V \sum_{\langle ij \rangle \xi \zeta \sigma \sigma'} n_{i\xi\sigma} n_{j\zeta\sigma'}, \quad (6)$$

with  $n_{i\xi\sigma} = \tilde{d}_{i\xi\sigma}^\dagger \tilde{d}_{i\xi\sigma}$ . This term reduces the probability of occupancy of neighboring sites by  $e_g$  electrons.

The form of the inter-site OO interactions included in the  $H_{OO}$  term of the Hamiltonian will be specified in the following section.

## B. Finite-temperature Lanczos method

To investigate the possible spin and orbital orderings in our spin-orbital model (1) we have calculated the temperature dependence of different two-site correlation functions given by the operator expectation value:

$$\langle A_{\mathbf{R}} \rangle = \frac{1}{Z} \sum_{n=1}^{N_{st}} \langle n | \exp(-\beta H) A_{\mathbf{R}} | n \rangle, \quad (7)$$

of two-site operators,  $A_{\mathbf{R}} = 1/N \sum_i B_i B_{i+\mathbf{R}}$  with  $B_i = n_i$ ,  $T_i^z$ ,  $S_i^z$ , or  $S_i^z n_i$  with  $n_i = \sum_{\xi\sigma} n_{i\xi\sigma}$ .<sup>46</sup> Here,  $\beta = 1/k_B T$ ,  $N_{st}$  is the number of basis states  $\{|n\rangle\}$  that span  $H$ ,  $N$  number of sites in the cluster and  $Z = \sum_{n=1}^{N_{st}} \langle n | \exp(-\beta H) | n \rangle$  is the partition function.

The calculation of (7) would, however, require a complete diagonalization of a  $N_{st} \times N_{st}$  matrix of the Hamiltonian. Therefore, we use for the calculation of  $\langle A_{\mathbf{R}} \rangle$

a generalization of the exact diagonalization technique developed by Jaklič and Prelovšek.<sup>47</sup> In this approach the trace of the thermodynamic expectation value is performed by a Monte Carlo sampling leading to the following approximate expression:

$$\langle A_{\mathbf{R}} \rangle \approx \frac{N_{st}}{LZ} \sum_{l=1}^L \sum_{j=1}^M \exp(-\beta E_j^l) \langle l | \psi_j^l \rangle \langle \psi_j^l | A_{\mathbf{R}} | l \rangle, \quad (8)$$

where the first sum is performed over a restricted number  $L$  of random states  $|l\rangle$  being initial states in the Lanczos algorithm to generate a set  $\{\psi_j^l\}$  of eigenfunctions of  $H$  with respective eigenvalues  $\{E_j^l\}$ .  $M$  is the number of Lanczos functions in the expansion of a given state  $|l\rangle$ . In the same manner the partition function is approximated by,

$$Z \approx \sum_{l=1}^L \sum_{j=1}^M \exp(-\beta E_j^l) |\langle l | \psi_j^l \rangle|^2. \quad (9)$$

It has been shown<sup>47</sup> that the results get very accurate already for  $L, M \ll N_{st}$ . Although we exploit the translational symmetry the calculations are restricted to small clusters ( $N = \sqrt{8} \times \sqrt{8}$  is used in this paper) as only  $S_{tot}^z = \sum_i S_i^z$  subspaces can be treated separately, while a similar symmetry in the orbital sector does not exist.

## III. NUMERICAL RESULTS

### A. Parameters and magnetic phases

In the numerical studies we assume  $S = 1/2$  for the core spins and the limit of strong Hund's coupling  $J_H/t = 15$ . The numerical results are almost identical for all  $J_H \gtrsim 5t$  in the whole range of temperatures considered by us. The Coulomb repulsion  $V/t$  and the AF-exchange  $J_{AF}/t$  are free parameters, and the data is summarized in form of a phase diagram in the  $V - J_{AF}$  plane. The hopping parameter  $t$  is chosen as energy unit. We focus in this study on CO states and thus assume finite positive values for  $V$  in all the calculations. In perovskite manganites the effective hopping  $t$  strongly depends on the lattice parameters and distortions *e.g.* increases with contraction of the Mn–O bond length and also depends on the Mn–O–Mn bond angle.<sup>3</sup> Thus, its value can be only roughly estimated as  $t = 0.2 - 0.7$  eV.<sup>41,48,49,50</sup>

A major difficulty when searching for spin structures like those indicated in Fig. 1, and the same applies to charge and orbital order, is that in a cluster with periodic boundary conditions translational (and rotational) symmetries are not broken. Therefore we have to investigate correlation functions and compare their features with the different spin configurations (presented in Fig. 1).

We shall consider three different forms for the orbital interaction term  $H_{OO}$  and show that one has to go beyond the nearest-neighbor interactions to obtain the CE-

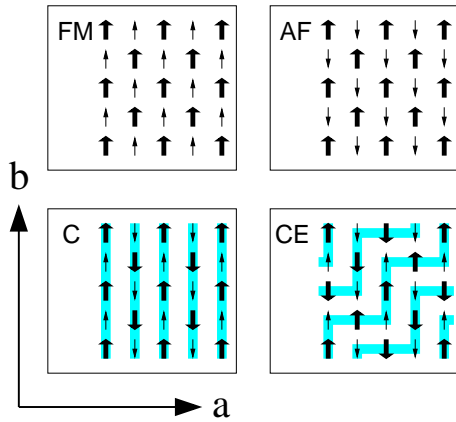


FIG. 1: Schematic view of different spin patterns found in the 2D model in presence of checkerboard CO (half-doped case). Thick (thin) arrows represent states with total spin  $S = 2$  ( $S = 3/2$ ) with (without) an  $e_g$  electron present at a given site, respectively. The shaded lines in C and CE phases indicate the direction of double exchange carrier propagation. The preferred directional  $e_g$  orbitals occupied at sites  $S = 2$  are parallel to the shaded paths.

type correlations. We begin the description of our calculations with a simplified model (without  $H_{OO}$  term) but including the crystal-field splitting of  $e_g$  orbitals  $\propto E_z$ ,

$$H_z = -E_z \sum_i T_i^z, \quad (10)$$

where  $T_i^z = \frac{1}{2} \sum_{\sigma} (n_{ix\sigma} - n_{iz\sigma})$  is the  $z$  component of the pseudospin operator. This orbital splitting accounts for the elongation of octahedra along the  $c$ -axis in layered compounds, which favors  $|z\rangle$  over  $|x\rangle$  orbital occupation, and also counterbalances the trend towards occupation of  $|x\rangle$  orbitals, which is strongly favored by the kinetic energy in the 2D-model. Although, the model without  $H_{OO}$  interactions can lead to the stability of the CE-type orbital pattern,<sup>46</sup> the magnetic structure was FM. In a wide range of parameters ( $E_z/t < 0$ ,  $V/t > 0$ ,  $J_{AF}/t > 0$ ) no stabilization of the AF CE spin phase was found, indicating that the inter-chain coupling is quite strong and cannot be neglected in realistic models for half-doped CO manganites. Such a conclusion agrees this recent density-functional calculations showing a considerable band dispersion normal to the chains.<sup>18</sup> Thus, we argue that the *topological effect* considered in 1D model approximations, which gave a simple explanation of the existence of the CE spin-orbital phase at half-doping, is not likely to be the decisive mechanism in a more realistic 2D case investigated here. Our simulations with purely electronic interactions do not provide evidence for 1D ferromagnetic chains that are coupled antiferromagnetically to neighbor chains, which is the basic assumption that could justify such 1D models. Therefore, in the following sections we concentrate on the electron-lattice coupling<sup>20,21,22,51,52</sup> and present a mechanism stabilizing the CE spin/orbital state in manganites.

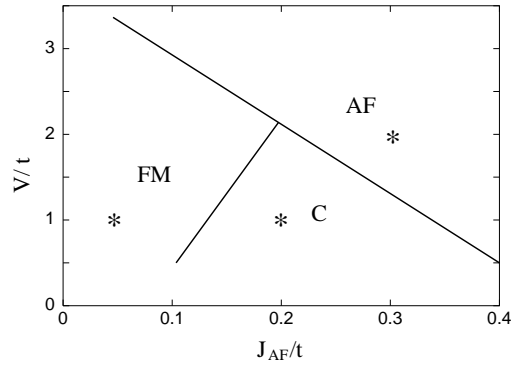


FIG. 2: Phase diagram indicating the character of the dominant spin correlations found at small temperatures  $T < zJ$ . The calculations include the nearest-neighbor OO effective interactions ( $\kappa = 0.2t$ ). '\*' indicates representative points for which the correlation functions are presented below.

## B. The role of nearest-neighbor orbital interactions

The first aim of our study of the spin-orbital model (1) in half-doped manganites is to investigate the role of nearest-neighbor OO coupling played in CO state. There are two different mechanisms contributing to this interaction: (i) the cooperative JT effect<sup>50</sup> and (ii) superexchange interactions.<sup>41,53</sup> Neglecting more complex spin-orbital terms<sup>49,50</sup> both effects can be described by the following simple term derived before for undoped LaMnO<sub>3</sub> compound,<sup>53</sup>

$$H_{OO} = 2\kappa \sum_{\langle ij \rangle} T_{ij}, \quad (11)$$

where the two-site orbital operator,  $T_{ij}$ , between nearest-neighbor Mn sites in the  $\{|x\rangle, |z\rangle\}$  basis,

$$T_{ij} = T_i^z T_j^z + 3T_i^x T_j^x \mp \sqrt{3}(T_i^x T_j^z + T_i^z T_j^x), \quad (12)$$

is described in terms of pseudospin operators:  $T_i^+ = \sum_{\sigma} \tilde{d}_{ix\sigma}^{\dagger} \tilde{d}_{iz\sigma}$ , and  $T_i^- = \sum_{\sigma} \tilde{d}_{iz\sigma}^{\dagger} \tilde{d}_{ix\sigma}$ . The prefactor of the mixed term  $\propto \sqrt{3}$  is negative in the  $a$  direction and positive in the  $b$  direction. The nearest-neighbor OO term can lead to *attraction* of electrons on neighboring sites with different orbital orientations but having the longer-range Coulomb repulsion (6) included in the model we avoid phase separation.

As shown in Fig. 2 for large values of the superexchange interaction between core spins ( $zJ_{AF} \sim t$ ) AF spin ground state is realized while with decreasing  $J_{AF}$  the kinetic energy of the  $e_g$  electrons ( $\sim t$ ) starts to play an active role via DE mechanism<sup>32</sup> breaking some of the AF bonds which leads to 1D FM chains which form straight lines (C phase). Further decrease of  $J_{AF}$  can give FM correlations in both  $a$  and  $b$  directions. As the kinetic energy is controlled by the inter-site Coulomb repulsion  $V$  and suppressed in the limit of  $V \gg t$  we find the AF region increasing in size with increasing  $V/t$ .

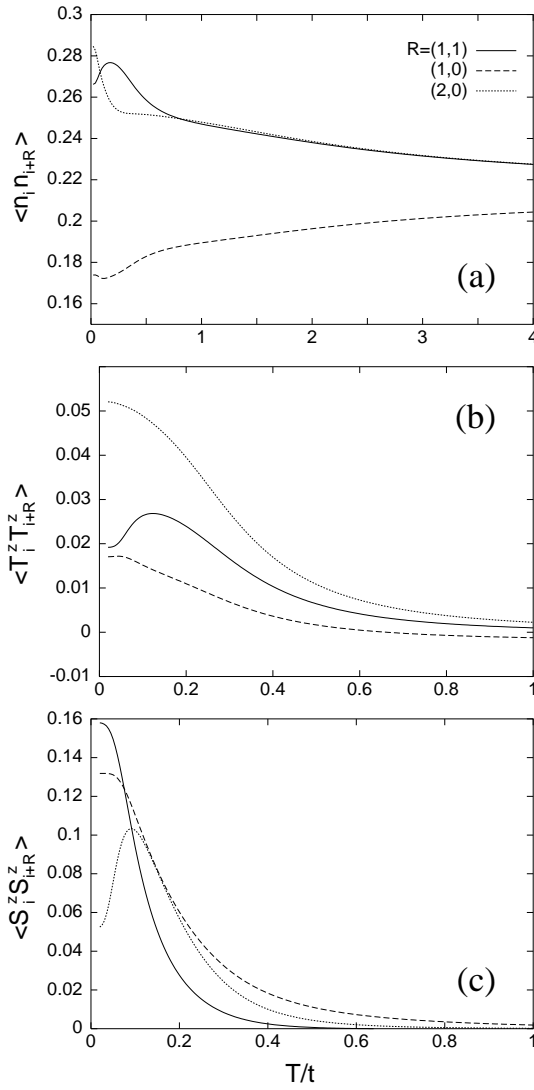


FIG. 3: Temperature dependence of the charge (a), orbital (b), and spin (c) two-site correlation functions calculated for neighbors at different distances  $\mathbf{R}$  for the phase with FM spin correlations. Parameters:  $V = t$ ,  $\kappa = 0.2t$ ,  $J_{AF} = 0.05t$ ,  $J_H = 15t$ .

We discuss now in more detail the temperature dependence of the different correlation functions. Starting from the FM region (see Fig. 3) we find the evolution of weak CO for  $T/t \lesssim 1$  with nearest-neighbor  $(1, 0)$  charge correlations smaller than the  $(1, 1)$  and  $(2, 0)$  next-neighbor ones which is consistent with the alternating order of  $\text{Mn}^{+3}$  and  $\text{Mn}^{+4}$  ions. The orbital correlations are positive between all neighbors indicating the preference of  $x^2 - y^2$  orbital occupancy due to the kinetic energy which is quite large in the FM state. Although all spin correlation functions are positive, they remain highly anisotropic as  $T \rightarrow 0$  as a result of the strong competition between the DE mechanism and AF superexchange interaction between core spins.

Next, we consider the AF spin state in the limit of

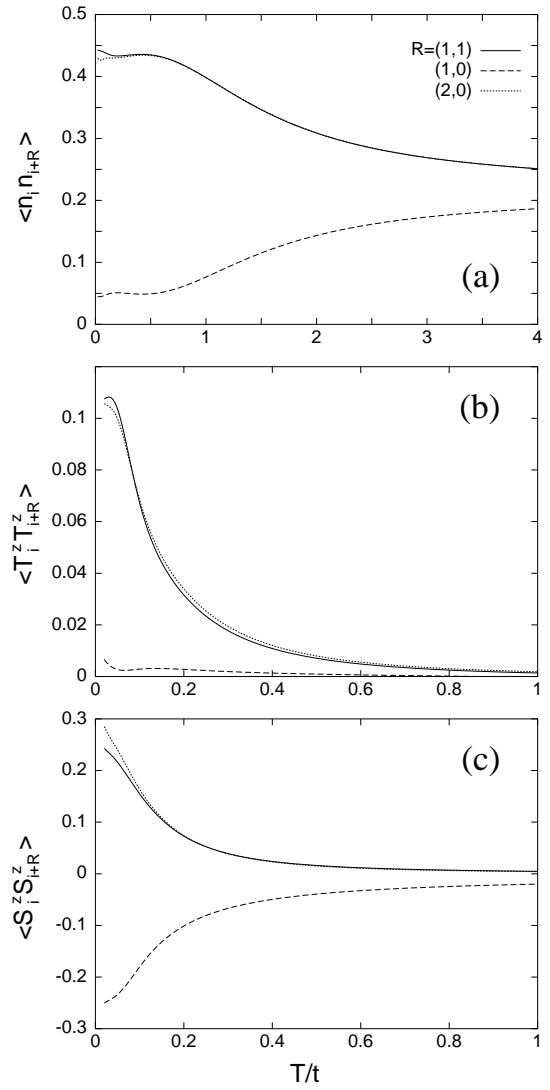


FIG. 4: Temperature dependence of the correlations as in Fig. 3 but for the phase with AF spin correlations. Parameters:  $V = 2t$ ,  $\kappa = 0.2t$ ,  $J_{AF} = 0.3t$ ,  $J_H = 15t$ .

larger both  $J_{AF}$  and  $V$  interactions (see Fig. 4). Increasing Coulomb repulsion ( $V = 2t$ ) we find more distinct and almost isotropic alternation of the  $e_g$  charge which now sets in already at  $T/t \approx 2$ . Here, the orbital correlations are strongly correlated with the onset of the AF spin order at  $T/t \approx 0.5$ . For  $T/t \rightarrow 0$  the spin-spin correlations are strong and represent an almost isotropic AF spin state.

For intermediate values of  $J_{AF}$  and moderate Coulomb repulsion we find the phase with predominantly C spin correlations at  $T/t \rightarrow 0$  (see Fig. 2). As presented in Fig. 5 for  $J_{AF}/t = 0.2$  and  $V/t = 1$  the charge correlations are similar to those obtained for the FM state shown in Fig. 3 (a) while the spin ordering change dramatically. Moreover for  $T/t \rightarrow 0$  the orbital correlations are weaker than those found in the FM state discussed above indicating the orbital tendency towards in-plane

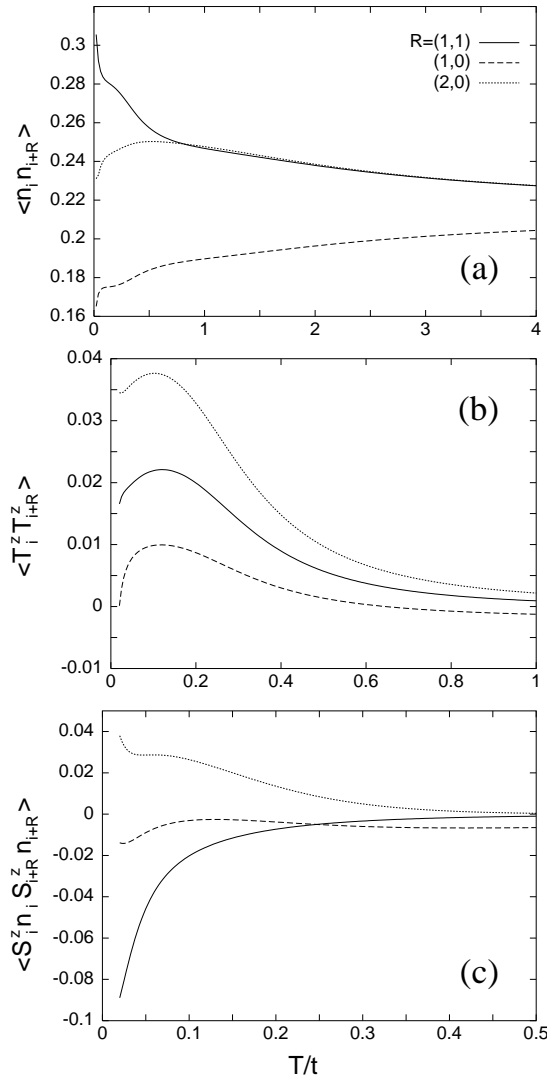


FIG. 5: Temperature dependence of the charge (a), orbital (b), and spin-charge (c) correlation functions calculated for the phase with C spin correlations. Parameters:  $V = t$ ,  $\kappa = 0.2t$ ,  $J_{AF} = 0.2t$ ,  $J_H = 15t$ .

directional-type order.

A convenient way to distinguish between phases with C or CE and other spin correlations is to evaluate a combined spin-charge correlation function being restricted to sites occupied by  $e_g$  electrons,  $\langle S_i^z n_i S_{i+R}^z n_{i+R} \rangle$ . Analyzing the localized limit presented in Fig. 1 (or its by  $\pi/2$  rotated version) one can easily see that, for the C phase one should find  $\langle S_i^z n_i S_{i+R}^z n_{i+R} \rangle > 0$  for  $|\mathbf{R}| = 2$  and  $\langle S_i^z n_i S_{i+R}^z n_{i+R} \rangle < 0$  for  $|\mathbf{R}| = \sqrt{2}$  while for the CE phase only  $\langle S_i^z n_i S_{i+R}^z n_{i+R} \rangle < 0$  for  $|\mathbf{R}| = 2$  with any other spin-charge correlations remaining small. In the case presented in Fig. 5  $\langle S_i^z n_i S_{i+R}^z n_{i+R} \rangle$  functions are negative (positive) for nearest-neighbors along diagonal (next-nearest-neighbors along  $a/b$  direction), respectively, in agreement with the arguments presented above. Furthermore, nearest-neighbor spin-charge correlations

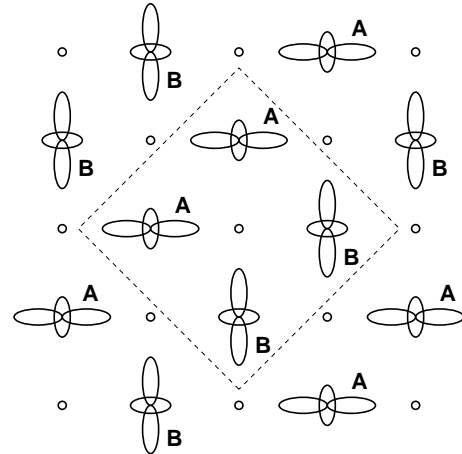


FIG. 6: Schematic configuration of the charge-orbital ordered CE phase. The sites **A** and **B** indicate two orbital  $Mn^{3+}$  sublattices while empty circles stand for the  $Mn^{4+}$  ions. The dashed-line box indicates a typical orbitals orientation around a given  $Mn^{4+}$  ion.

are small as a result of averaging over different cluster orientations (rotated by angles  $\pm\pi/2$ ,  $\pm\pi$ ).

It is easy to see why the C-structure is favored by the nearest-neighbor JT interaction. The C-phase can be viewed as a realization of the alternating orbital structure of  $LaMnO_3$  but with a modulated charge density. Hence this structure is compatible with the nearest-neighbor JT interaction, whereas in the CE-structure this interaction is frustrated.

### C. Elastic interactions

The role of local lattice distortions due to JT effect, which creates an anisotropic strain field decaying as  $\sim R^{-3}$ , in promoting long-range orbital ordering was considered by Khomskii (see Ref. 39). Following these arguments, we treat the OO term as an elastic interaction which is active also between  $e_g$  electrons on next-nearest-neighbor sites along  $a$  or  $b$  direction,

$$H_{el} = 2\kappa \sum_{\langle ij \rangle} T_{ij} + 2\kappa' \sum_{\langle\langle ij \rangle\rangle} T_{ij}, \quad (13)$$

where  $\langle\langle ij \rangle\rangle$  refers to next nearest-neighbors along  $a$  and  $b$  direction with  $\kappa' = \kappa/8$  which follows from the  $\sim (|i-j|)^{-3}$  decay of elastic interactions.<sup>39</sup> The existence of longer-range OO interactions is justified by its cooperative lattice-driven nature where an orbital flip on a single Mn site distorts not only the neighboring oxygens but also positions of other manganese ions around it. Here, the JT coupling preferring the tilting of the orbitals from the uniform orbital state leads to an alternating orbital order (see Fig. 6) and in this way compensates for the kinetic energy gain in uniform  $|x\rangle$  orbital state favored in the 2D model.

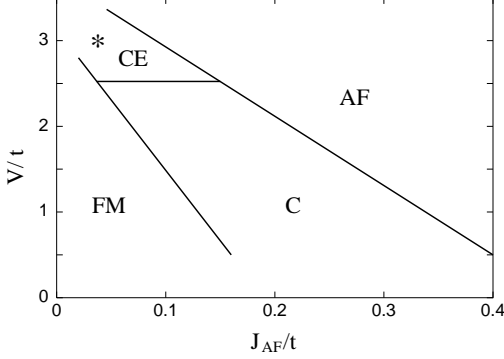


FIG. 7: Phase diagram as in Fig. 2 including the nearest- and next-neighbor elastic interactions ( $\kappa = 0.2t$ ,  $\kappa' = \kappa/8$ ). '\*' indicates a representative point in the CE region for which the correlation functions are presented here.

The CE phase is favored as compared to the C phase by the OO coupling between second neighbors ( $\sim \kappa'$ ) along  $a/b$  direction. However, this interaction is only active (not screened) when strong charge ordering takes place (large  $V/t$  limit) and here the CE phase can persist even for small values of  $J_{AF}$  as long as the  $e_g$  kinetic energy is sufficiently suppressed by a large  $V$  (see Fig. 7). Thus, one has to assume large inter-site Coulomb repulsion (where almost perfect  $Mn^{+3}/Mn^{+4}$  charge ordering<sup>6</sup> is realized) and small superexchange interaction [see an example for  $V/t = 3$  and  $J_{AF}/t = 0.04$  in Fig. 8]. In the  $\{|x\rangle, |z\rangle\}$  basis, which we use in most of the numerical evaluations, the spin and orbital correlation functions with  $\mathbf{R} = (2, 0)$  become large as  $T \rightarrow 0$  while all the others remain very small in the whole range of temperatures. Such small orbital correlations imply either that the respective orbitals are uncorrelated or that they order in such a way, that the occupied orbitals are linear combinations with almost equal amplitude expressed in the basis used for the measurement of correlation functions.<sup>41</sup> This difficulty is not present in SU(2) symmetric models, and appears here as consequence of the cubic symmetry in the orbital sector. Therefore, the same functions were evaluated also in the  $\{(|x\rangle \pm |z\rangle)/\sqrt{2}\}$  basis as presented in the inset of Fig. 8 (b). In the new orbital basis the function  $\langle T_i^z T_{i+(2,0)}^z \rangle$  is more pronounced and saturates for  $T/t \simeq 0.1$  at  $\langle T_i^z T_{i+(2,0)}^z \rangle \simeq -0.12$  close to its maximum value  $-1/8$  indicating almost perfect CE orbital structure (see Fig. 6). Shorter range  $\langle T_i^z T_{i+\mathbf{R}}^z \rangle$  correlations should become small when averaged over differently oriented clusters (rotated by angles  $\pm\pi/2$ ) [see Fig. 1 (d)]. From Fig. 1 (d) one can see that a similar pattern as found for the two-site orbital correlations should be found for the  $\langle S_i^z n_i S_{i+\mathbf{R}}^z n_{i+\mathbf{R}} \rangle$  functions. In our cluster in ideal CE state only electrons at distance  $|\mathbf{R}| = 2$  can contribute to the charge-spin correlations (being negative in this case) which do not vanish when averaged over different cluster orientations. As shown in Fig. 8 (c) the  $\langle S_i^z n_i S_{i+\mathbf{R}}^z n_{i+\mathbf{R}} \rangle$  correlations obtained

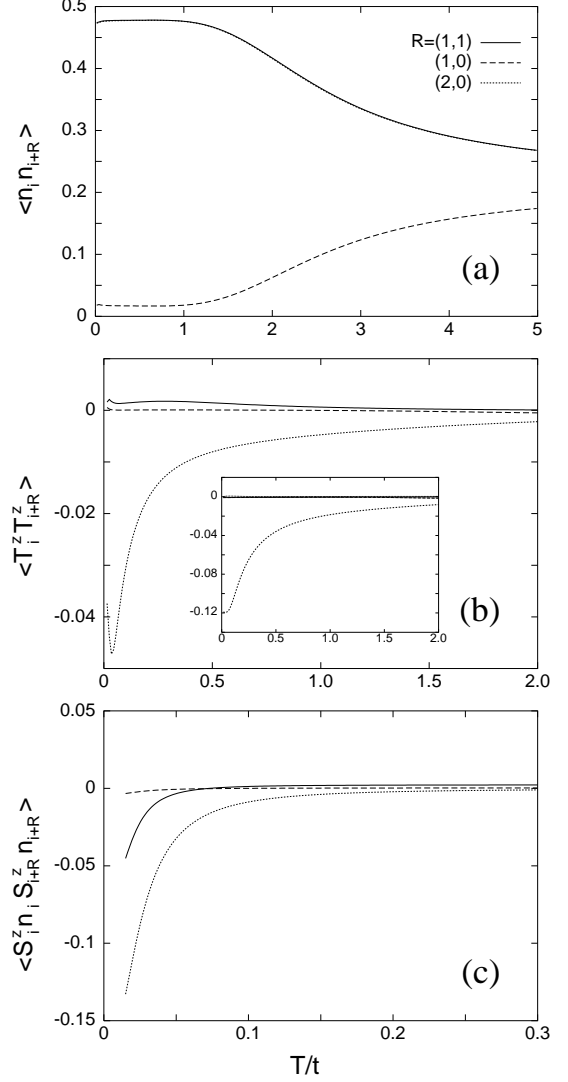


FIG. 8: Temperature dependence of the two-site correlations as in Fig. 5 but for the phase with CE spin and orbital correlations promoted by elastic interactions ( $\kappa = 0.2t$ ,  $\kappa' = \kappa/8$ ). Other parameters:  $V = 3t$ ,  $J_{AF} = 0.04t$ ,  $J_H = 15t$ . The inset in (b) shows the orbital correlations in the rotated basis:  $\{(|x\rangle \pm |z\rangle)/\sqrt{2}\}$ .

here are consistent with the above characterization of the CE pattern with a strong negative signal dominating at distance  $|\mathbf{R}| = 2$ . The existence of charge-ordered insulating state concomitant with orbital and spin order of the CE-type<sup>10,11</sup> was observed in different half-doped manganites with small one-electron bandwidth.<sup>1</sup>

The average change in the orbital occupation can be studied calculating  $\langle T_i^z \rangle$  which changes between  $+1/4$  and  $-1/4$  for the uniform  $|x\rangle$  and  $|z\rangle$  orbital states, respectively, for the case with one  $e_g$  electron per two Mn sites. Furthermore, when the orbital state involves  $|x\rangle$  and  $|z\rangle$  orbitals in the same proportion one finds  $\langle T_i^z \rangle \simeq 0$ . In Fig. 9 (a) we see that increasing the Coulomb interaction from  $V = t$  to  $V = 2t$  the orbital or-

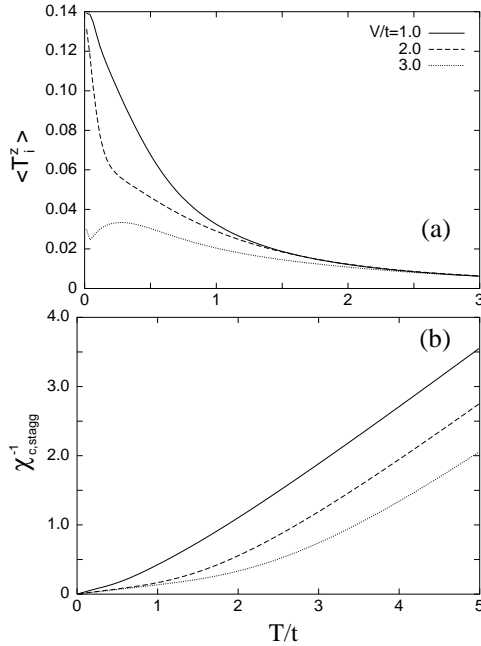


FIG. 9: Temperature dependence of the average value of the  $T_i^z$  orbital operator (a) and the inverse of the staggered charge susceptibility  $\chi_{c,stagg}^{-1}$  (b) obtained for different values of the inter-site repulsion  $V/t$  in the presence of elastic interactions ( $\kappa = 0.2t$ ,  $\kappa' = \kappa/8$ ). Other parameters:  $J_{AF} = 0.04t$ ,  $J_H = 15t$ .

dering hardly changes for  $T/t \rightarrow 0$  with  $\langle T_i^z \rangle$  only slightly decreasing to  $\langle T_i^z \rangle \simeq 0.13$  for  $V = 2t$ . This indicates that as long as the system is in the FM state (see Fig. 7) the ground state is dominated by the  $x^2 - y^2$  orbital promoted by the kinetic energy term. Further increase in the Coulomb inter-site repulsion to  $V = 3t$  leads to a drastic change in the orbital order when system enters the CE phase region (see Fig. 7). Here,  $\langle T_i^z \rangle \simeq 0.03$  for  $T/t \rightarrow 0$  indicating dominating role played by the  $(|x\rangle \pm |z\rangle)/\sqrt{2}$  orbitals. This fact is consistent with our results for the two-site orbital correlation functions [see inset in Fig. 8(b)].

A change in the inter-site Coulomb interaction is directly connected with the robustness of the charge ordering as seen in Figs. 3 - 5 (a) and Fig. 8 (a). Although the characteristic temperature of the charge order ( $T_{CO}$ ) can be roughly estimated from the charge-charge correlation functions it can be more precisely extracted from the staggered charge susceptibility,<sup>46</sup>  $\chi_{c,stagg}$ :

$$\chi_{c,stagg} = \beta/N \sum_{ij} (-1)^{|i-j|} \langle \left( n_i - \frac{1}{2} \right) \left( n_j - \frac{1}{2} \right) \rangle, \quad (14)$$

which at high temperatures follows a Curie-Weiss law  $\chi_{c,stagg}^{-1} \propto (T - T_{CO})$ . From Fig. 9 (b) one can easily estimate  $T_{CO}/t \approx 0.6$ , 1.4, and 2.4 for  $V/t = 1.0$ , 2.0, and 3.0, respectively, in agreement with the mean-field solution<sup>54</sup> which for  $V \gg t$  predicts,  $T_{CO} \approx zV/4$ .

#### D. Local Mn<sup>3+</sup>–Mn<sup>3+</sup> JT interactions

Although the model considered in the previous section with longer-range OO elastic coupling leads to the CE-type spin and orbital correlations, this phase is found only in a very extreme case of almost perfect Mn<sup>4+</sup>/Mn<sup>3+</sup> CO (that is for strong Coulomb repulsion) which may not be very realistic in the light of some experimental facts indicating the CDW character of charge redistribution between different manganese ions.<sup>31</sup> Therefore in this section we derive the further neighbor OO interactions from a microscopic model including apart from the JT-distortion of the Mn<sup>3+</sup> octahedra the breathing distortion around the Mn<sup>4+</sup> ions as well. We then show that this interaction is capable to produce the zigzag (spin and orbital) phase in a region of small Coulomb repulsion changing the previous phase diagrams in a drastic way.

To assess the gain in lattice energy connected with the formation of the CE long-range orbital order we follow the work of Millis for LaMnO<sub>3</sub> by treating the lattice distortions classically.<sup>55,56</sup> The effect of lattice displacements is treated assuming arbitrary values of four different lattice distances  $d_i$  ( $i = 1, \dots, 4$ ) (see Fig. 10) which are expressed by  $\delta_x$ ,  $\delta'_x$  – uniform deformation along the  $a$  and  $b$  direction of the Mn lattice, and  $u_i$  – displacements of O ions along the Mn–O–Mn bonds within the  $(a, b)$  planes:

$$d_1 = \frac{1}{2}b(1 + \delta_x - 2u_1), \quad (15a)$$

$$d_2 = \frac{1}{2}b(1 + \delta_x + 2u_1), \quad (15b)$$

$$d_3 = \frac{1}{2}b(1 + \delta'_x + 2u_2), \quad (15c)$$

$$d_4 = \frac{1}{2}b(1 + \delta'_x - 2u_2), \quad (15d)$$

where  $b$  is the lattice constant of the ideal perovskite. Moreover, we assume the  $e_g$  charge stacking in the  $c$  direction with the respective Mn–Mn distance being  $b(1 + \delta_z)$ .

In order to define orbital sublattices (A and B) we introduce a transformation which describes the tilting of orbitals by making two different transformations at both sublattices,<sup>53</sup>

$$\begin{bmatrix} |i\mu\rangle \\ |i\nu\rangle \end{bmatrix} = \begin{bmatrix} \cos\left(\frac{\pi}{4} \pm \phi\right) & \sin\left(\frac{\pi}{4} \pm \phi\right) \\ -\sin\left(\frac{\pi}{4} \pm \phi\right) & \cos\left(\frac{\pi}{4} \pm \phi\right) \end{bmatrix} \begin{bmatrix} |iz\rangle \\ |ix\rangle \end{bmatrix}, \quad (16)$$

where  $-$  ( $+$ ) refers to  $i \in A$  ( $i \in B$ ) sublattice, respectively, and  $|\phi| \leq \frac{\pi}{4}$ . Here,  $|ix\rangle$  and  $|iz\rangle$  stands for local basis orbitals:  $|x\rangle$  and  $|z\rangle$  at site  $i$ , respectively. In the rotated basis  $\{|i\mu\rangle, |i\nu\rangle\}$  we assume for the transformed operators:  $\langle T_i^z \rangle = -1/2$  ( $1/2$ ) for  $i \in A$  ( $B$ ) sublattice, respectively. At intermediate values of  $\phi$  one can reach, e.g.,  $|3x^2 - r^2\rangle/|3y^2 - r^2\rangle$  ( $|z^2 - x^2\rangle/|z^2 - y^2\rangle$ )-type orbital ordering at  $\phi = \pi/12$  ( $\phi = -\pi/12$ ), respectively. The rotation (16) does not include complex orbital order which

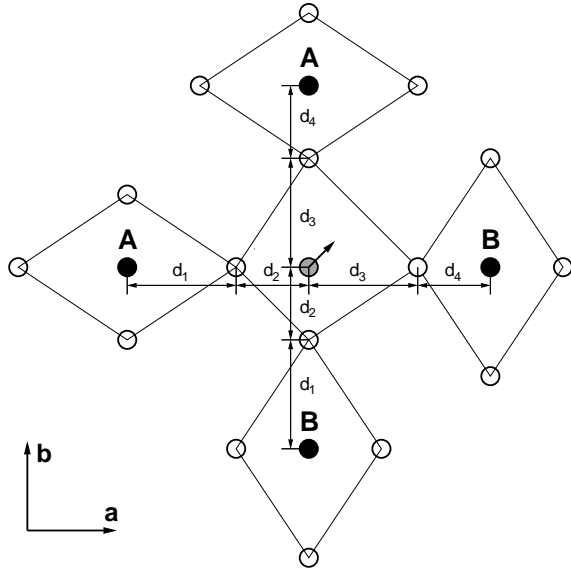


FIG. 10: Schematic representation of the lattice distortions contributing to the second neighbor JT-interaction. The corresponding CE orbital order for the 5 atom structure above is indicated in Fig. 6 by dashed lines. Different  $\text{Mn}^{3+}$ ,  $\text{Mn}^{4+}$ , and O ions are presented by full, shaded and empty circles, respectively. The distances between the  $\text{Mn}^{4+}$  ion and the  $\text{Mn}^{3+}$  ions in (10) [ $(\bar{1}0)$ ] and (01) [ $(0\bar{1})$ ] directions, respectively, are identical. The arrow indicates the displacement of the central  $\text{Mn}^{4+}$  ion when  $d_1 + d_2 \neq d_3 + d_4$ .

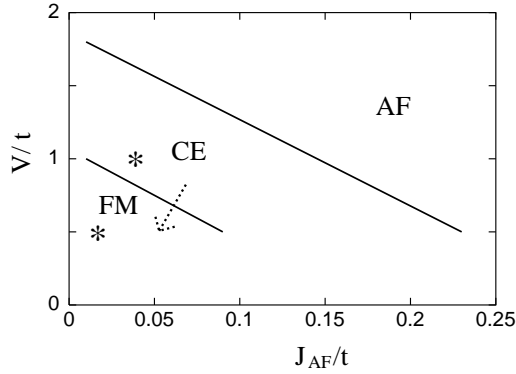


FIG. 11: Phase diagram as in Fig. 2 including the local nearest- and next-neighbor OO interactions with  $\kappa = 0.2t$  and  $\kappa' = 0.1t$  (spring constants  $K_2/K_1 = 0.25$ ). '\*' indicate representative points in the CE region for which the correlation functions are presented here. The dashed arrow presents the direction of the transition from the localized CE to the itinerant electron A-phase at low temperatures.

was proposed as a possible orbital order in manganites at smaller doping.<sup>57</sup> The classical energy of the distorted lattice  $E_l$  (per Mn site) is given by,<sup>56</sup>

$$E_l = \frac{1}{4} (K_1 + 2K_2) [\delta_x^2 + (\delta'_x)^2 + \delta_z^2] + K_1 (u_1^2 + u_2^2), \quad (17)$$

normalized per Mn ion, where  $K_1$  ( $K_2$ ) are the nearest-

neighbor Mn–O (Mn–Mn) spring constant, respectively.

Next, we have to add the energy of the breathing mode (BM) describing the attraction between oxygen ions and the unoccupied  $\text{Mn}^{4+}$  site:

$$E_{br} = \frac{1}{2} \beta \lambda (\delta_x + \delta'_x + \delta_z + u_1 + u_2). \quad (18)$$

Here, all oxygens are equally attracted towards the central manganese ion. The BM induces charge alternation on neighboring Mn sites and contributes to the effective inter-site charge-charge repulsion ( $V$ ). The coupling constant to the breathing distortion is written as  $\beta\lambda$ , where  $\lambda$  denotes the coupling to the JT distortion. The term describing the JT coupling depends on the character of the occupied orbital at a  $\text{Mn}^{3+}$  site. The JT interaction describes the coupling between the occupied  $e_g$  orbital at a particular  $\text{Mn}^{3+}$  ion and the distortions of the surrounding oxygen ions, as introduced by Millis.<sup>55</sup> In the orbitally rotated state (16) this energy has the following form,

$$E_{JT}(\phi) = \frac{1}{2} \lambda \left\{ \left[ \delta_z + u_1 + u_2 - \frac{1}{2} (\delta_x + \delta'_x) \right] \sin(2\phi) - \sqrt{3} \cos(2\phi) \left[ \frac{1}{2} (\delta_x - \delta'_x) + u_2 - u_1 \right] \right\}, \quad (19)$$

and depends on the rotation angle  $\phi$  and on the deformation of the lattice.

The optimal values of the ionic displacements for a given angle  $\phi$  are found by minimization of the total energy,  $E_{tot}(\phi) = E_l + E_{br} + E_{JT}(\phi)$ , which for (17)–(19) and neglecting higher-order nonlinear terms gives,

$$\delta_x = \frac{-\lambda [2\beta - \sin(2\phi) - \sqrt{3} \cos(2\phi)]}{2(K_1 + 2K_2)}, \quad (20a)$$

$$\delta'_x = \frac{-\lambda [2\beta - \sin(2\phi) + \sqrt{3} \cos(2\phi)]}{2(K_1 + 2K_2)}, \quad (20b)$$

$$\delta_z = \frac{-\lambda [\beta + \sin(2\phi)]}{K_1 + 2K_2}, \quad (20c)$$

$$u_1 = \frac{-\lambda [2\beta + \sin(2\phi) + \sqrt{3} \cos(2\phi)]}{4K_1}, \quad (20d)$$

$$u_2 = \frac{-\lambda [2\beta + \sin(2\phi) - \sqrt{3} \cos(2\phi)]}{4K_1}. \quad (20e)$$

This yields for the total energy of the distorted lattice,

$$E_{tot}(\phi) = -\frac{\lambda^2}{4K_1(K_1 + 2K_2)} \left\{ \beta^2 (5K_1 + 4K_2) + (K_1 + 2K_2) [2\beta \sin(2\phi) + \cos^2(2\phi)] + 2K_1 + K_2 \right\}. \quad (21)$$

This implies a change of the volume of the lattice with respect to the ideal perovskite ( $V_0 = b^3$ )  $\delta V/V_0 \simeq \delta_x + \delta'_x + \delta_z = -3\lambda\beta/(K_1 + 2K_2)$ . Hence the volume decreases with increasing BM coupling  $\beta$ , but does not depend on the character of the orbital order.

TABLE I: The relative energy gain,  $\delta E(\phi)/E_{tot}(\phi)$ , associated with the  $\text{Mn}^{4+}$  ion displacement (see Fig. 10) for the orbital orderings given by  $\phi = 0$  and  $\pm\pi/12$  presented as function of  $\beta$  and  $K_2/K_1$ .

$\beta$	$K_2/K_1$	$\phi = \pi/12$	$\phi = 0$	$\phi = -\pi/12$
		$\delta E(\phi)/E_{tot}(\phi)$	$\delta E(\phi)/E_{tot}(\phi)$	$\delta E(\phi)/E_{tot}(\phi)$
0.0	0.0	0.409	0.500	0.409
1.0	0.0	0.167	0.187	0.129
2.0	0.0	0.054	0.065	0.045
0.0	0.5	0.281	0.333	0.281
1.0	0.5	0.125	0.130	0.087
2.0	0.5	0.040	0.046	0.031
0.0	1.0	0.214	0.250	0.214
1.0	1.0	0.100	0.100	0.065
2.0	1.0	0.032	0.036	0.024

The relative strength of the effective next- and nearest-neighbor JT interactions can be obtained by comparing the lattice stiffnesses of the orbital modulations in the undoped ( $\sim \kappa$ ) and the quarter-filled ( $\sim \kappa'$ ) case, respectively. For *undoped*  $\text{LaMnO}_3$  the lattice energy was found to be [see Eq. (2.14) in Ref. 58],

$$E_{tot}^0(\phi) = -\frac{3\lambda^2}{K_1(K_1 + 2K_2)} \{K_1 + K_2[1 + \cos(4\phi)]\}, \quad (22)$$

while in the half-doped case the orbital alternation on  $\text{Mn}^{3+}$  sites is driven by the  $\text{Mn}^{4+}$  ion shift lowering the distorted lattice energy by,

$$\delta E(\phi) = -\frac{3\lambda^2}{16(K_1 + 2K_2)} [1 + \cos(4\phi)], \quad (23)$$

being *independent* of the strength of the BM. Contrary to the undoped case (22), where the Mn-Mn potential ( $\sim K_2$ ) is necessary to obtain finite orbital stiffness, in the half-doped case (23) the Mn-O interaction alone can lead to cooperative JT effect stabilizing the alternating orbital order. Assuming  $\lambda = 6\text{eV}$ ,  $K_1 = 200\text{ eV}$ , and  $0 < K_2/K_1 < 1$  (see Ref. 55) one finds for the  $|x\rangle \pm |z\rangle$  ( $\phi = 0$ ) orbital order the CE energy contribution per Mn ion  $\delta E \simeq 20 - 70\text{ meV}$ .

In Table I we presented the ratio  $\delta E(\phi)/E_{tot}(\phi)$ , characterizing the stability of the CE orbital order, as function of the BM coupling strength  $\beta$  and the ratio of spring constants  $K_2/K_1$ . The largest relative gain in energy due to the  $\text{Mn}^{4+}$  ions shift ( $\sim b|\delta_x - \delta'_x|$ ) is obtained for the  $(|x\rangle + |z\rangle)/(|x\rangle - |z\rangle)$  orbital order ( $\phi = 0$ ) which for small BM coupling ( $\sim \beta$ ) can reach up to 50% of the total lattice energy, whereas for larger values of  $\beta$ , although  $\delta E(\phi)$  is not changed, the total lattice energy increases rapidly as  $\sim \beta^2$  being dominated by the distortions of the  $\text{MnO}_6$  octahedra rather than by their displacements. Furthermore, with increasing Mn lattice stiffness ( $\sim K_2/K_1$ ) both  $\delta E(\phi)/E_{tot}(\phi)$  ratio and the shift of unoccupied  $\text{Mn}^{4+}$  ions [ $\sim \lambda/(K_1 + 2K_2)$ ] decreases.

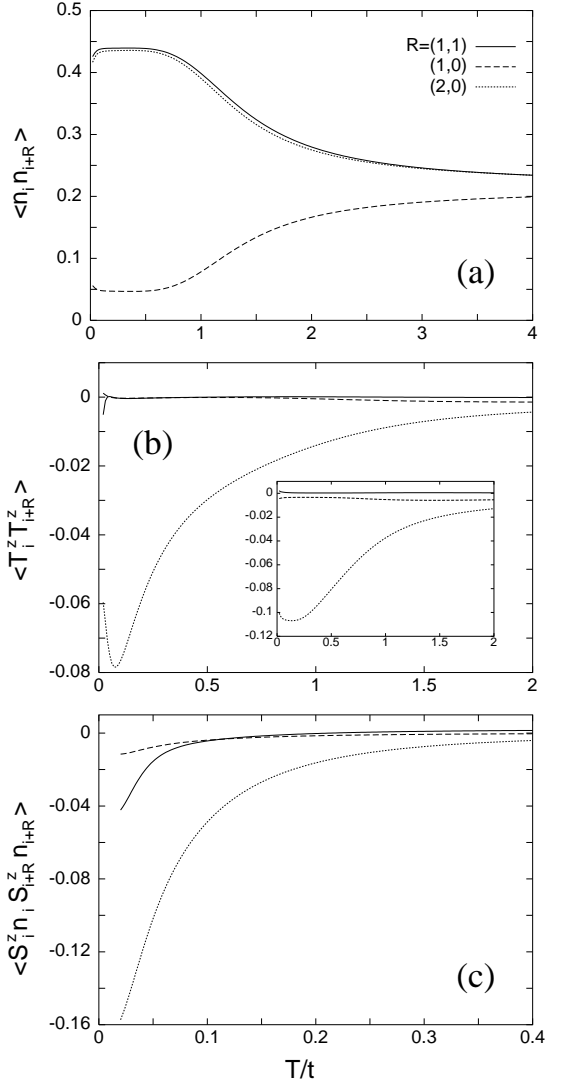


FIG. 12: Correlation functions in the case of a CE ground state (as in Fig. 8) but obtained for the local OO interaction (26) with spring constants  $K_2/K_1 = 0.25$  ( $\kappa' = \kappa/2$ ). Other parameters:  $V = t$ ,  $\kappa = 0.2t$ ,  $J_{AF} = 0.04t$ ,  $J_H = 15t$ .

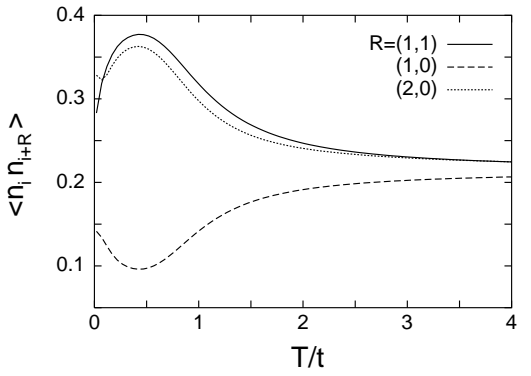


FIG. 13: Charge correlations in the case of a FM ground state as obtained for the local OO interaction with spring constants  $K_2/K_1 = 0.25$  ( $\kappa' = \kappa/2$ ). Other parameters:  $V = 0.5t$ ,  $\kappa = 0.2t$ ,  $J_{AF} = 0.02t$ ,  $J_H = 15t$ .

Comparing the cooperative part [ $\sim \cos(4\phi)$ ] of both JT energy contributions [(22) and (23)] we end up with a simple relation between different OO interaction strengths,

$$\frac{\kappa'}{\kappa} = \frac{K_1}{8K_2}. \quad (24)$$

For  $K_2 = K_1$  the  $\sim R^{-3}$  scaling of elastic interactions<sup>39</sup> is recovered. In the above estimate we have neglected the superexchange interaction which can also contribute to the effective  $\kappa$  [see *e.g.* Eq. (2.7) in Ref. 58].

The relative strength of both spring constants in the CO case can be assessed from the relative length of different bonds in the half-doped  $\text{MnO}_2$  plane. As measured for low-temperature  $\text{La}_{0.5}\text{Ca}_{0.5}\text{MnO}_3$  superstructure<sup>38</sup> the length of all four in-plane  $\text{Mn}^{4+}$ -O bonds is very similar ( $d_2 = d_3 \simeq 1.915\text{\AA}$ ). Neglecting the effect of Mn-O-Mn bond bending and assuming  $d_2 \simeq d_3$  (see Fig. 10) one obtains the relation,

$$K_2 \ll K_1, \quad (25)$$

by using Eqs. (20). The above assessment together with (24) underlines the importance of  $\text{Mn}^{3+}$ - $\text{Mn}^{3+}$  orbital coupling ( $\sim \kappa'$ ) in CO manganites. Moreover, the length of  $\text{Mn}^{3+}$ -O in-plane bonds<sup>38</sup> ( $d_1 \simeq 2.07\text{\AA}$  and  $d_4 \simeq 1.92\text{\AA}$ ) measured in  $\text{La}_{0.5}\text{Ca}_{0.5}\text{MnO}_3$  at  $T < T_N$  leads to an approximate value of the strength of the BM coefficient,  $\beta \simeq 1.8$ . This implies that the energy gain due to the breathing distortion is substantial [see Eq.(21)].

As the OO interaction between further  $\text{Mn}^{3+}$  neighbors is mediated by an  $\text{Mn}^{4+}$  ion we propose the following effective three-site interaction,

$$H'_{\text{OO}} = 2\kappa' \sum_{\langle\text{ijj}'\rangle} (1 - n_{\text{j}}) T_{\text{ijj}'}, \quad (26)$$

where the operator  $T_{\text{ijj}'}$  is defined as in Eq.(12), and  $\langle\text{ijj}'\rangle$  denotes three neighboring sites along  $a$  or  $b$  direction. The OO coupling of the form (26) will lead to the pattern of stable bi-stripes observed<sup>59</sup> in  $\text{La}_{1-x}\text{Ca}_x\text{MnO}_3$  at commensurate carrier concentrations (*e.g.*  $x = 2/3, 3/4, 4/5$ ) while the Wigner-crystal arrangement<sup>60</sup> would be preferred at large values of inter-site Coulomb repulsion.

Investigating the model (1) with both nearest-neighbor (11) and three-site (26) OO couplings we find a strong change in the low-temperature phase diagram (see Fig. 11) as compared with the previous ones (Figs. 2 and 7). Assuming  $\kappa' = \kappa/2$  (which corresponds to  $K_2/K_1 = 1/4$ ), the CE-like correlations set in already at rather small inter-site repulsion ( $V \simeq 0.5t$ ) while for stronger Coulomb interactions ( $V \gtrsim 1.5t$ ) the spin correlations have predominantly AF character. Furthermore, the FM region is quite small and can be found only for  $V \lesssim t$  and  $J_{\text{AF}} \lesssim 0.1t$ . When decreasing the ratio  $K_2/K_1$  (and keeping the value of  $\kappa'$  constant) the FM region shrinks at the expense of the CE region.

Next, we present the two-site correlations for one representative ( $V = t$ ,  $J_{\text{AF}} = 0.04t$ ) point in the CE region in Fig. 11. From Fig. 12 (a) one sees that the CE state can exist for less pronounced CO than in the elastic strain model considered in Sec. III C, where almost perfect  $\text{Mn}^{3+}/\text{Mn}^{4+}$  CO was necessary to stabilize the zigzag state (see Fig. 8). Moreover, the evolution of CE-type orbital order with decreasing temperature is here correlated with the onset of CO [compare Fig. 12 (a)-(b) with 8 (a)-(b)]. Regarding  $\langle S_{\text{i}}^z n_{\text{i}} S_{\text{i}+\text{R}}^z n_{\text{i}+\text{R}} \rangle$  correlations, the CE-type spin order develops at lower temperatures than the charge and orbital order but at higher temperature than previously found for the strain induced interactions. The three-site term (26) which is active for a  $\text{Mn}^{3+}$ - $\text{Mn}^{4+}$ - $\text{Mn}^{3+}$  sequence along the  $a$  and  $b$  direction, respectively, promotes not only orbital alternation on neighboring  $\text{Mn}^{3+}$  sites but also strengthens CO. This is clearly seen in the charge correlations which are now stronger than those *e.g.* in Fig. 3, although the same Coulomb repulsion ( $V = t$ ) was assumed in both cases.

Going from the CE to the FM phase (as indicated by an arrow in Fig. 11) one finds that the CDW is now reduced at low temperatures in the FM state (Fig. 13), while the charge modulation is still rather strong at higher temperatures ( $T/t \approx 0.5$ ) above the Néel temperature where the electron kinetic energy is quenched due to the random  $t_{2g}$  spin orientations. This behavior is a clear manifestation of the double exchange mechanism. We note that the CE-type orbital correlations are still present in the FM phase in Fig. 11 for  $V \gtrsim 0.5t$ , whereas for smaller values for  $V$   $x^2-y^2$  orbital correlations dominate, which are characteristic for the metallic A-phase.

## E. Charge modulation in the $c$ direction

Finally, we consider possible mechanisms stabilizing the charge stacking of CE-ordered planes<sup>61</sup> as observed in most charge-ordered manganites at doping  $x = 1/2$ . Any interaction stabilizing such a stacking must overcome the inter-site charge-charge repulsion. There are two interactions which contribute to such a repulsion: (i) the electron-electron Coulomb force  $V$ ; and (ii) the BM coupling. Both interactions will effectively tend to maximize the number of  $\text{Mn}^{3+}$ - $\text{Mn}^{4+}$  bonds. The BM coupling contribution to the inter-site charge-charge repulsion ( $V_{\text{BM}}$ ) can be estimated comparing the lattice energies with charge alternating and stacked along the  $c$  direction which leads to the estimate  $V_{\text{BM}} = \lambda^2 [2\beta - \sin(2\phi)]^2 / (16K_1)$ . Assuming typical values for  $\lambda = 10t$  and  $K_1 = 500t$  (see Ref. 55) together with our previous estimate  $\beta \simeq 1.8$  one can obtain *e.g.*  $V_{\text{BM}} \simeq 0.16t$  for the  $\{|x\rangle \pm |z\rangle\}/\sqrt{2}$  CE orbital order.

In a multi-layer system the OO interaction along the  $c$  direction is given by the nearest-neighbor coupling  $\sim \kappa$ ,

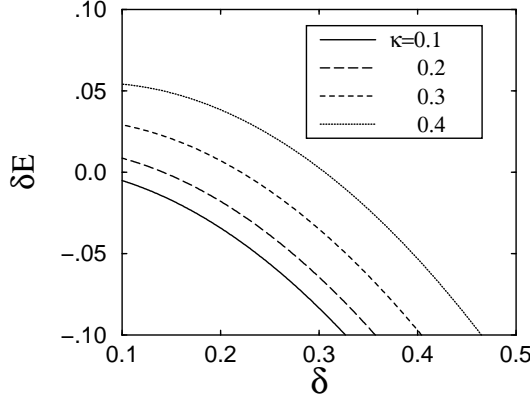


FIG. 14: Energy gained by  $e_g$  electron stacked in the  $c$  direction as function of charge modulation  $\delta$  obtained for  $V = 0.5t$ ,  $\kappa' = 0.1t$  and different values of  $\kappa$ .

which in the  $\{|x\rangle, |z\rangle\}$  basis has the form,<sup>53</sup>

$$H_{OO}^c = 8\kappa \sum_{\langle ij \rangle c} T_i^z T_j^z. \quad (27)$$

This interaction together with the  $\sim \kappa'$  coupling, which controls the CE-orbital order in the  $(a, b)$  plane, in a charge-ordered case yields an approximate orbital model of the form,

$$H_{OO} \simeq 6\kappa' \sum_{\langle ij \rangle ab} T_i^z T_j^z + 8\kappa \sum_{\langle ij \rangle c} T_i^x T_j^x. \quad (28)$$

where  $T_i^z$  ( $T_i^x$ ) are defined with respect to the  $\{|(x) \pm (z)\}/\sqrt{2}\}$  orbital basis. Defining  $|\pm\rangle \equiv (|x\rangle \pm |z\rangle)/\sqrt{2}$  and assuming that in the  $(a, b)$  planes of a bilayer system  $|+\rangle_i$  and  $|+\rangle_j$  orbitals are occupied on two neighboring sites in the  $c$  direction, the  $\sim \kappa$  coupling [see Eq. (28)] rotates orbitals towards the  $|-\rangle_i \otimes |-\rangle_j$  configuration and leads to binding of two electrons with energy  $E_b = \sqrt{(12\kappa')^2 + 4\kappa^2} - 12\kappa'$ . For charge disproportion with  $Mn^{3.5 \pm \delta}$  ions alternating in the  $(a, b)$  planes and assuming that the  $\kappa$  ( $\kappa'$ ) two (three)-site interaction scales as  $\sim (1/2 + \delta)^\alpha$  with  $\alpha = 2$  (3), respectively, one can obtain the energy gain (per Mn ion) by charge stacked in the  $c$  direction which for the 3D lattice is,

$$\delta E = 6\kappa' \left( \frac{1}{2} + \delta \right)^3 \left[ \sqrt{1 + \frac{\kappa^2}{36\kappa'^2(\frac{1}{2} + \delta)^2}} - 1 \right] - 2\delta^2 V. \quad (29)$$

The last term stands for the effective Coulomb repulsion at given charge modulation. With charge modulation sufficiently reduced  $\delta \sim 0.2 - 0.3$  (see Fig. 14) the OO inter-plane coupling can stabilize charge-stacked phase ( $\delta E > 0$ ). Such stabilization is strengthened (weakened) by increasing  $\kappa$  ( $\kappa'$ ) OO interaction, respectively. For smaller charge disproportion ( $\delta \lesssim 0.1$ ) and considerable charge on  $Mn^{3.5 - \delta}$  sites the  $\sim \kappa$  in-plane coupling [neglected in Eq. (28)] can also play an important role in the

inter-plane charge modulation. However, when the CO is strongly reduced the orbital ground state is too complex to be analyzed analytically.

A further mechanism stabilizing the observed  $e_g$  charge stacking along the  $c$  direction results from the AF inter-plane superexchange interaction<sup>20</sup>. Yet, the magnetic interaction ( $J_{AF}$ ) results mainly from the  $t_{2g} - t_{2g}$  superexchange which is of the order of only a few meV.<sup>50</sup> Thus, the antiferromagnetism in the  $c$  direction observed in most of the CE structures is a *result* rather than the *origin* of the stacking pattern of the charge/orbital order.

#### IV. SUMMARY

We have investigated the potential of different electron-lattice mechanisms to stabilize the CE spin-orbital ordered phase in charge ordered half-doped manganites (filled with one  $e_g$  electron per two Mn ions). Our study is based on a generalized DE model containing the  $e_g$  orbital degrees of freedom, and also including inter-site Coulomb repulsion ( $V$ ) and AF superexchange ( $J_{AF}$ ) between core spins. The effect of three types of orbital interactions derived from the cooperative JT effect have been studied: (i) nearest neighbor JT-coupling, which is responsible for the alternating orbital order in undoped  $LaMnO_3$ , (ii) in addition second neighbor JT-interaction with a strength as expected for elastic strain, and (iii) a 2nd neighbor JT interaction which accounts for the breathing distortion of the  $Mn^{4+}$  octahedra and is in general stronger than (ii). A particular feature of this interaction, which has been derived from a microscopic model in Sec. III D, are the displacements of the  $Mn^{4+}$  ions in the CE-phase.

We have studied these models employing finite temperature diagonalization on a  $\sqrt{8} \times \sqrt{8}$  cluster with periodic boundary conditions, thereby keeping the translational invariance. The evolution of the different phases with temperature is monitored by the calculation of correlation functions for charge, orbital and spin, respectively. Starting out from the generalized ferromagnetic Kondo lattice model (1) without any orbital interaction ( $H_{OO} = 0$ ) we find the orbital correlations dominated by the  $x^2 - y^2$  orbitals which are favored by the kinetic energy.<sup>41,42</sup> This orbital state is characteristic for the metallic A-phase in wide-band manganites at half doping. For small AF superexchange interactions ( $J_{AF} \ll t$ ) between  $t_{2g}$  core spins the FM state is found in the spin sector, while for larger values of  $J_{AF}$  the ground state is that of a regular 2 sublattice antiferromagnet. Even for large Coulomb repulsion  $V$  we found no evidence for C or CE structures for some intermediate values of the parameter  $J_{AF}$ . The inclusion of the nearest-neighbor JT-interaction (i), however, was found to stabilize the AF-C phase in a wide parameter range in the  $V - J_{AF}$  phase diagram.

To obtain the more complex CE orbital and spin state not only the kinetic energy must be reduced by increas-

ing the Coulomb repulsion  $V$  but also a further neighbor *antiferro-orbital* interaction must be included in the model. This interaction results from the electron-lattice coupling and is a generalization of the JT interaction which was found to play an important role in the parent  $\text{LaMnO}_3$  compound.<sup>55,56</sup> In CO compounds at quarter-filling the effect of the OO coupling will be dominated by interactions between further distant Mn neighbors. We have shown that such interactions can produce the CE structure in both *spin and orbital* sectors. In the case of the three-site effective interaction ( $\sim \kappa'$ ) the zigzag chains are found to be stable not only for modest inter-site repulsion ( $V \simeq 0.5t$ ) but even in the limit of  $V = 0$  and provided  $\kappa$  is small, where the CO is induced entirely by the three-site orbital coupling (26). This effective next-nearest-neighbor OO coupling was derived taking into account the cooperative nature of both  $\text{Mn}^{3+}$ –O and  $\text{Mn}^{3+}$ – $\text{Mn}^{4+}$  bonds length deformation. The free relaxation of the latter length leads in presence of CO to orbital alternation in planar directions, and the pattern of directed orbitals typical for the orbital CE structure appears. Consequently, with the help of the orbital topology,<sup>12,13</sup> this gives rise to the CE antiferromagnetic spin ordering for realistic values for  $J_{\text{AF}}$ .

An important aspect of the second neighbor JT-interaction (iii) is its 3-site structure which involves a coupling to the charge at the  $\text{Mn}^{4+}$  ion. This implies that the evolution of the CE orbital correlations with temperature are linked to the evolution of CO, while the magnetic CE correlations develop at lower temperature similar to  $\text{Pr}_{1/2}\text{Ca}_{1/2}\text{MnO}_3$ <sup>34,35</sup>. This is different from (ii), where first CO develops, then OO and finally at lowest temperature AF spin order.

As discussed in Sec. III A we did not find the CE spin and/or orbital phase considering a pure electronic model, i.e., neglecting the electron-lattice coupling. Although, the topological effect combined with the DE mechanism leads to the preference of the CE over C phase when all  $e_g$  (bridge and corner) orbitals are degenerate,<sup>13</sup> the situation is more complex when such degeneracy is lifted by JT lattice distortions. As described in the Appendix, one finds band insulators in both cases while the stability of the CE versus the C phase strongly depends on the crystal-field splittings ( $E_z, \eta E_z \sim \lambda$ ).

An important issue is the degree of charge ordering in the CE phase. The CE spin-orbital structures obtained in our simulations appear in the regime of relatively strong CO, as inferred from our calculated charge correlation functions. Our calculations also suggest that the second neighbor JT coupling even for small or vanishing Coulomb repulsion can lead to a pronounced charge modulation. These results are consistent with the simple physical picture, that DE perpendicular to the FM chains must be strongly suppressed to allow AF superexchange to trigger the CE structure, which may not be the case for weak CO. On the other hand a recent study by Mahadevan, Terakura and Sarma<sup>62</sup> based on the band structure approach arrived at the conclusion that the charge dif-

ference between the two Mn species in the CE phase is basically negligible, which would imply the absence of a significant breathing distortion of  $\text{Mn}^{4+}$  octahedra. Further experimental information on the degree of lattice distortion in the CE phase will certainly help to test the proposed JT based mechanism for the stability of the CE phase.

The charge modulations determined in our calculations may be influenced by numerical limitations which overestimate quantum fluctuations: (i) spins  $S = 1/2$  are used to describe  $t_{2g}$  electrons; (ii) the calculations are made using a 2D cluster; (iii) the oxygen ions are not present explicitly in the cluster and thus only *dynamical* interactions are included ( $\kappa, \kappa'$ ), which are mediated by oxygen displacements, while possible *static* lattice effects<sup>63</sup> are neglected. Certainly each of these approximations weakens the charge ordering and the spin-orbital order. It is, however, not straightforward to decide whether the region of the CE-phase in the phase diagram may grow or shrink, if quantum fluctuations are suppressed.

Finally we note that further neighbor JT interactions can also play an important role in the charge stripe formation at other commensurate carrier concentrations. For  $x < 1/2$  ( $x > 1/2$ ) the dominant coupling arises from the nearest- (next nearest-) neighbor OO interactions, respectively, with a pronounced electron-hole asymmetry present. In the latter case with small inter-site Coulomb repulsion ( $V$ ) the bi-stripe state<sup>59</sup> would be preferred while larger values of  $V$  would favor a “Wigner crystal” charge arrangement.<sup>60</sup>

## Acknowledgments

We would like to thank G. Khaliullin, M. Mayr and A. M. Oleś for stimulating discussions and valuable comments. J. B. acknowledges the support of the MPI für Festkörperforschung, Stuttgart. The financial support by the Polish State Committee of Scientific Research (KBN) of Poland, Project No. 5 P03B 055 20 is also acknowledged (J. B.).

## APPENDIX: 1D BAND MODEL

A quite appealing explanation for the stability of the CE as compared to the C phase was suggested in Refs.12,13 by considering a 1D model, where in the CE phase a gap opens as a consequence of a topological sign in the hopping matrix-elements. However, the intra-site Coulomb repulsion  $U$  (leading to some redistribution of the  $e_g$  charge) can destabilize the CE phase.<sup>64,65</sup> Here we investigate how these arguments are modified when orbital degeneracy is lifted due to JT distortions. We consider the Hamiltonian:

$$H^{1\text{D}} = H_t + E_{z(b)} \sum_{i \in \text{corner}} T_i^z + \frac{1}{2} \eta E_{z(b)} \sum_{i \in \text{bridge}} n_i, \quad (\text{A.1})$$

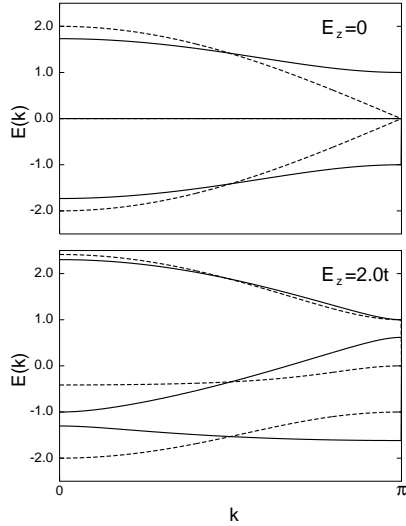


FIG. 15: Electron dispersion for the zigzag chain of the CE phase (solid lines) and for the linear chain of the C phase (dashed lines) calculated for different crystal-field splittings in the  $\{|x\rangle, |z\rangle\}$  orbital basis at corner sites ( $E_z$ ). The orbitals at the bridge sites are degenerate (assuming  $\eta = 0$ ).

which contains the kinetic energy  $H_t$  of an electron hopping along a FM chain<sup>13</sup> with possible  $e_g$  level shift at the bridge sites ( $\propto \eta E_{z(b)}$ ) and level splitting at corner sites ( $\propto E_{z(b)}$ ) considered in two different orbital basis  $\{|x\rangle, |z\rangle\}$  and  $\{|a\rangle = \frac{1}{\sqrt{2}}(|x\rangle + |z\rangle), |b\rangle = \frac{1}{\sqrt{2}}(|x\rangle - |z\rangle)\}$ . We assume that the energies of the bridge  $3x^2 - r^2/3y^2 - r^2$  orbitals are located between the split energy levels at the corners assuming  $|\eta| \leq 1$ . Both kinds of level shifts can result from the lattice distortions. At the bridge site only the orbital  $3x^2 - r^2$  ( $3y^2 - r^2$ ) is considered while the orthogonal one  $y^2 - z^2$  ( $x^2 - z^2$ ), respectively, is decoupled in chain direction. In momentum space this leads to a  $3 \times 3$  matrix problem:

$$H^{1D} = \sum_k \begin{pmatrix} d_{B,k}^\dagger \\ d_{x,k}^\dagger \\ d_{z,k}^\dagger \end{pmatrix}^T \begin{bmatrix} \eta E_z & W'_k & W_k \\ W'_k & E_z & 0 \\ W_k & 0 & -E_z \end{bmatrix} \begin{pmatrix} d_{B,k} \\ d_{x,k} \\ d_{z,k} \end{pmatrix}, \quad (\text{A.2})$$

where  $W_k = -2t \cos k$  ( $2t \cos k$ ) and  $W'_k = -2\sqrt{3}t \sin k$  ( $2\sqrt{3}t \cos k$ ) are the hopping elements for the CE (C) phase, respectively, in the  $\{|x\rangle, |z\rangle\}$  orbital basis.

Calculating the band energies (see Fig. 15) one can easily determine the character of the stable phase. For the degenerate band model ( $E_z = 0$ ) the C phase is metallic while in the CE phase a gap opens due to the *topological sign*.<sup>12,13</sup> The opening of the gap stabilizes the CE phase. When the degeneracy between  $|x\rangle$  and  $|z\rangle$  states at the corner sites ( $E_z \neq 0$ ) is lifted, the C phase becomes insulating as well and for sufficiently large  $e_g$  level splittings it can have a *lower* energy than the CE phase when the

chain is doped with one electron per two Mn sites [see Fig. 15(b)]. The region of stability of the CE phase in-

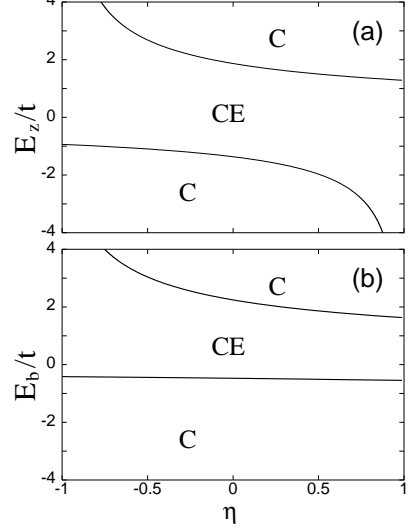


FIG. 16: Phase diagram of the chain model illustrating the stability of the CE against the C phase as function of the crystal-field splittings defined with respect to the orbital basis (a)  $\{|x\rangle, |z\rangle\}$  and (b)  $\{\frac{1}{\sqrt{2}}(|x\rangle \pm |z\rangle)\}$ , respectively.

creases for positive (negative)  $E_z$  when  $\eta \rightarrow -1(1)$ , respectively [see Fig. 16(a)]. Generally, the CE phase is stabilized with respect to C, when the occupied bridge state approaches the lower energy level of the corner states. In a real half-doped crystal where in the CE phase Mn–O bond lengths shrink (expand) in the  $c$  direction [ $(a, b)$  plane], respectively, one would expect an energetic preference, due to the JT effect, for orbitals with stronger  $x^2 - y^2$  than  $3z^2 - r^2$  character. Thus, in the 1D model the relevant part of the phase diagram (Fig. 16) is the region with  $E_z < 0$  and  $\eta E_z < 0$ , i.e., where the CE structure dominates.

To relate our mean-field considerations to the model from Sec. III B the stability of the CE phase versus C was also considered with level splitting at the corner sites defined with respect to the orbital basis  $\{\frac{1}{\sqrt{2}}(|x\rangle \pm |z\rangle)\}$ . Such a splitting, directly related to the nearest-neighbor JT interaction (11) when  $E_b > 0$ , is operative in the C phase but vanishes by symmetry in the CE orbital phase. As shown in Fig. 16(b) the CE phase is stable for small splittings ( $0 \lesssim E_b \lesssim 2t$ ) and in the  $E_b > 0$ ,  $\eta \rightarrow -1$  region. The latter is the relevant parameter range in the case of nearest neighbor JT interactions, and hence the model suggests the CE phase as stable phase. This, however, is in conflict with our numerical study of the 2D model, where only the C phase was found to be stable. As in 2D the nearest neighbor JT interaction stabilizes the C structure, whereas this interaction is frustrated in the CE phase. This effect is not included in the 1D model.

<sup>1</sup> For a review see: M. Imada, A. Fujimori, and Y. Tokura, Rev. Mod. Phys. **70**, 1039 (1998).

<sup>2</sup> Y. Tokura and N. Nagaosa, Science **288**, 462 (2000).

<sup>3</sup> Y. Moritomo, H. Kuwahara, Y. Tomioka, Y. Tokura, Phys. Rev. B **55**, 7549 (1997).

<sup>4</sup> R. Kajimoto, H. Yoshizawa, Y. Tomioka, and Y. Tokura, Phys. Rev. B **66**, 180402 (2002).

<sup>5</sup> B. J. Sternlieb, J. P. Hill, U. C. Wildgruber, G. M. Luke, B. Nachumi, Y. Moritomo, and Y. Tokura, Phys. Rev. Lett. **76**, 2169 (1996).

<sup>6</sup> Y. Murakami, H. Kawada, H. Kawata, M. Tanaka, T. Arima, Y. Moritomo, and Y. Tokura, Phys. Rev. Lett. **80**, 1932 (1998).

<sup>7</sup> K. Nakamura, T. Arima, A. Nakazawa, Y. Wakabayashi, and Y. Murakami, Phys. Rev. B **60**, 2425 (1999).

<sup>8</sup> R. Kilian and G. Khaliullin, Phys. Rev. B **60**, 13 458 (1999).

<sup>9</sup> K. I. Kugel and D. I. Khomskii, Zh. Eksp. Teor. Fiz. **64**, 1429 (1973) [Sov. Phys. JETP **37**, 725 (1973)]; Usp. Fiz. Nauk **136**, 621 (1982) [Sov. Phys. Usp. **25**, 232 (1982)].

<sup>10</sup> J. B. Goodenough, Phys. Rev. **100**, 564 (1955).

<sup>11</sup> E. O. Wollan and W. C. Koehler, Phys. Rev. **100**, 545 (1955).

<sup>12</sup> I. V. Solovyev and K. Terakura, Phys. Rev. Lett. **83**, 2825 (1999).

<sup>13</sup> J. van den Brink, G. Khaliullin, and D. Khomskii, Phys. Rev. Lett. **83**, 5118 (1999).

<sup>14</sup> I. V. Solovyev, Phys. Rev. B **63**, 174406 (2001).

<sup>15</sup> T. Mutou and H. Kontani, Phys. Rev. Lett. **83**, 3685 (1999).

<sup>16</sup> G. Jackeli, N. B. Perkins, and N. M. Plakida, Phys. Rev. B **62**, 372 (2000).

<sup>17</sup> Z. Shu, J. Dong, and D. Y. Xing, Phys. Rev. B **63**, 224409 (2001).

<sup>18</sup> Z. Popović and S. Satpathy, Phys. Rev. Lett. **88**, 197201 (2002).

<sup>19</sup> T. Mizokawa and A. Fujimori, Phys. Rev. B **56** R493 (1997).

<sup>20</sup> S. Yunoki, T. Hotta, and E. Dagotto, Phys. Rev. Lett. **84**, 3714 (2000).

<sup>21</sup> T. Hotta, Y. Takada, H. Koizumi, and E. Dagotto, Phys. Rev. Lett. **84**, 2477 (2000).

<sup>22</sup> T. Hotta, A. Feiguin, and E. Dagotto, Phys. Rev. Lett. **86**, 4922 (2001).

<sup>23</sup> R. Y. Gu and C. S. Ting, Phys. Rev. B **65**, 214426 (2002).

<sup>24</sup> Y. Tomioka, A. Asamitsu, Y. Moritomo, H. Kuwahara, and Y. Tokura, Phys. Rev. Lett. **74**, 5108 (1995).

<sup>25</sup> H. Kawano, R. Kajimoto, H. Yoshizawa, Y. Tomioka, H. Kuwahara, and Y. Tokura, Phys. Rev. Lett. **78**, 4253 (1997).

<sup>26</sup> M. v. Zimmermann, C. S. Nelson, J. P. Hill, Doon Gibbs, M. Blume, D. Casa, B. Keimer, Y. Murakami, C.-C. Kao, C. Venkataraman, T. Gog, Y. Tomioka, and Y. Tokura, Phys. Rev. B **64**, 195133 (2001).

<sup>27</sup> M. Kubota, H. Yoshizawa, Y. Moritomo, H. Fujioka, K. Hirota, and Y. Endoh, J. Phys. Soc. Jpn **68**, 2202 (1999).

<sup>28</sup> D. N. Argyriou *et al.*, Phys. Rev. B **61**, 15269 (2000).

<sup>29</sup> S. Ishihara and S. Maekawa, Phys. Rev. B **62**, 5690 (2000).

<sup>30</sup> C. H. Chen, S. Mori, and S.-W. Cheong, Phys. Rev. Lett. **83**, 4792 (1999).

<sup>31</sup> S. Laroche, A. Mehta, N. Kaneko, P. K. Mang, A. F. Panchula, L. Zhou, J. Arthur, and M. Greven, Phys. Rev. Lett. **87**, 095502 (2001).

<sup>32</sup> C. Zener, Phys. Rev. **82**, 403 (1951); P. W. Anderson and H. Hasegawa, Phys. Rev. **100**, 675 (1955).

<sup>33</sup> T. Hotta, A. L. Malvezzi, and E. Dagotto, Phys. Rev. B **62**, 9432 (2000).

<sup>34</sup> H. Kajimoto, H. Yoshizawa, Y. Tomioka, and Y. Tokura, Phys. Rev. B **63**, 212407 (2001).

<sup>35</sup> M. v. Zimmermann *et al.*, Phys. Rev. Lett. **83**, 4872 (1999).

<sup>36</sup> J. Geck, D. Bruns, C. Hess, R. Klingeler, P. Reutler, M. v. Zimmermann, S.-W. Cheong, and B. Büchner, Phys. Rev. B **66**, 184407 (2002).

<sup>37</sup> A. Moreo, S. Yunoki, and E. Dagotto, Science **283**, 2034 (1999).

<sup>38</sup> P. G. Radaelli, D. E. Cox, M. Marezio, and S.-W. Cheong, Phys. Rev. B **55**, 3015 (1997).

<sup>39</sup> D. I. Khomskii and K. I. Kugel, Europhys. Lett. **55**, 208 (2001); D. I. Khomskii, Int. J. Mod. Phys. **15**, 2665 (2001).

<sup>40</sup> M. J. Calderon, A. J. Millis, and K. H. Ahn, cond-mat/0305440.

<sup>41</sup> P. Horsch, J. Jaklič, and F. Mack, Phys. Rev. B **59**, 6217 (1999).

<sup>42</sup> F. Mack and P. Horsch, Phys. Rev. Lett. **82**, 3160 (1999).

<sup>43</sup> M. Uehara, S. Mori, C. H. Chen, and S.-W. Cheong, Nature **399**, 560 (1999).

<sup>44</sup> Y. Okimoto *et al.*, Phys. Rev. B **59**, 7401 (1999).

<sup>45</sup> J. H. Jung *et al.*, Phys. Rev. B **62**, 481 (2000).

<sup>46</sup> F. Mack, Ph. D. thesis, Max-Planck-Institut für Festkörperforschung, Stuttgart, 1999.

<sup>47</sup> J. Jaklič and P. Prelovšek, Adv. Phys. **49**, 1 (2000).

<sup>48</sup> A. E. Bocquet, T. Mizokawa, T. Saitoh, H. Namatame, and A. Fujimori, Phys. Rev. B **46**, 3771 (1992); T. Saitoh, A. E. Bocquet, T. Mizokawa, H. Namatame, A. Fujimori, M. Abbate, Y. Takeda, and M. Takano, *ibid.* **51**, 13 942 (1995); S. Satpathy, Zoran S. Popovic and Filip R. Vukajlovic, Phys. Rev. Lett. **76**, 960 (1996).

<sup>49</sup> S. Ishihara, J. Inoue, and S. Maekawa, Phys. Rev. B **55**, 8280 (1997).

<sup>50</sup> L. F. Feiner and A. M. Oleš, Phys. Rev. B **59**, 3295 (1999).

<sup>51</sup> A. J. Millis, Nature **392**, 147 (1998).

<sup>52</sup> J. Bała, A. M. Oleš, and G. A. Sawatzky, Phys. Rev. B **65**, 184414 (2002).

<sup>53</sup> J. van den Brink, P. Horsch, F. Mack, and A. M. Oleš, Phys. Rev. B **59**, 6795 (1999).

<sup>54</sup> U. Yu, Y. V. Skrypnyk, and B. I. Min, Phys. Rev. B **61**, 8936 (2000).

<sup>55</sup> A. J. Millis, Phys. Rev. B **53**, 8434 (1996).

<sup>56</sup> K. H. Ahn and A. J. Millis, Phys. Rev. B **58**, 3697 (1998).

<sup>57</sup> J. van den Brink and D. I. Khomskii, Phys. Rev. B **63**, 140416 (2001); R. Maezono and N. Nagaosa, *ibid.* **62**, 11 576 (2000).

<sup>58</sup> J. Bała, A. M. Oleš, and P. Horsch, Phys. Rev. B **65**, 134420 (2002).

<sup>59</sup> S. Mori, C. H. Chen, and S.-W. Cheong, Nature **392**, 473 (1998).

<sup>60</sup> P. G. Radaelli, D. E. Cox, L. Capogna, S.-W. Cheong, M. Marezio, Phys. Rev. B **59**, 14440 (1999).

<sup>61</sup> Deviations from this rule are observed when Re and A cations order; see T. Arima *et al.*, Phys. Rev. B **66**, 140408 (2002).

<sup>62</sup> P. Mahadevan, K. Terakura, and D. D. Sarma, Phys. Rev.

Lett. **87**, 066404 (2001).  
<sup>63</sup> J. Bała and A. M. Oleś, Phys. Rev. B **62**, 6085 (2000).  
<sup>64</sup> S.-Q. Shen, Phys. Rev. Lett. **86**, 5842 (2001).  
<sup>65</sup> M. Cuoco, C. Noce, and A. M. Oleś, Phys. Rev. B **66**, 094427 (2002).